DOI: 10.24874/ti.2263.06.26.10

Tribology in Industry

www.tribology.rs

RESEARCH

Failure Analysis of Premature Fracture in Cone Crusher Mantle Liners Used in Iron Ore Crushing

Maria Luisa Couy Viana[a], Wivyan Castro Lage[a], Fabrício Vieira de Andrade[a], Tarcisio Gonçalves de Brito[a], Gustavo Tressia[b,*]

[a]*Universidade Federal de Itajubá, Departamento de Engenharia de Materiais, Itabira, Minas Gerais, Brazil,*
[b]*Instituto Tecnológico Vale, Ouro Preto, Minas Gerais, Brazil.*

Keywords:

Hadfield steel
Wear
Failure analysis
Quaternary crushing
Crusher liners

* Corresponding author:

Gustavo Tressia
E-mail: gustavo.tressia@itv.org

Received:
Revised:
Accepted:

A B S T R A C T

This study analyzed three premature failures occurring in crusher mantle liners made from Hadfield steel (ASTM A128/A128M Grade C) used in quaternary crushing of iron ore. All failures followed a similar pattern, characterized by premature crack formation and catastrophic fracture after a short operating time, which is unexpected behavior for high-manganese austenitic steel. Mechanical tests and characterization analyses—optical emission spectroscopy, optical microscopy, scanning electron microscopy, tensile tests, impact tests, and hardness tests—were performed on samples extracted from the crack initiation regions. Results indicate deviations in chemical composition compared to ASTM A128/A128M Grade C, particularly in chromium and manganese content, in addition to grain-boundary carbide precipitation and micro-shrinkage defects, which may reduce local grain-boundary cohesion and facilitate crack initiation. Mechanical testing revealed reduced mechanical performance, while bulk hardness measurements near the crack-initiation regions did not permit a definitive assessment of surface work hardening developed during service, suggesting improper alloy composition and microstructural defects from the foundry process. Mitigating actions are proposed to prevent recurrence of similar failures.

© 2026 Published by Faculty of Engineering

1. INTRODUCTION

Comminution is a fundamental stage in mineral processing, responsible for reducing particle size to levels that allow the adequate liberation of valuable minerals from gangue minerals in iron ore beneficiation. This process is typically carried out through multiple stages—crushing and grinding—depending on ore hardness, mineral associations, and the required product specifications. Among the different crushing equipment used in the industry, cone crushers play a central role in secondary, tertiary, and particularly quaternary crushing stages, producing feed material suitable for subsequent grinding circuits [1].

In cone crushers, the mantle and concave are subjected to intense abrasive wear due to the continuous interaction between the iron ore particles and the steel surfaces. This wear mechanism is predominantly governed by three-body abrasion, in which free particles roll and slide between two solid bodies, promoting material removal from the liner surfaces [1]. To withstand such harsh tribological conditions, industries extensively employ Hadfield steel (ASTM A128/A128M [2]), an austenitic manganese steel widely used because of its ability to combine impact toughness with excellent resistance to abrasive wear through work-hardening.

Despite its well-established mechanical performance, unexpected premature failures of Hadfield steel mantle liners are still reported in industrial practice. These failures can lead to unplanned shutdowns, decreased equipment availability, elevated maintenance costs, and reduced operational efficiency. Premature failures are generally associated with metallurgical deficiencies, including improper alloy chemistry, inadequate heat treatment, or microstructural defects introduced during casting. These factors can reduce austenite stability and impair the work-hardening response required for satisfactory performance in crushing applications [3,4].

In this context, the present study investigates three premature failures in CH660 cone crusher mantle liners used in quaternary iron ore comminution. While the expected operational lifetime is approximately 800 hours, the analyzed liners failed at 260, 375, and 560 hours, respectively. The objective of this study is to identify the root causes of premature mantle-liner failures through chemical, microstructural, mechanical, and fractographic characterization. The findings are used to establish the dominant failure mechanisms and propose corrective actions for manufacturing and quality-control processes.

2. MATERIALS AND METHODS

2.1 Materials

In this study, mantle liners procured and specified for service as ASTM A128/A128M Grade C [2] austenitic manganese steel were analyzed after exhibiting premature failure (Figure 1) during service in CH660 cone crushers used in the quaternary crushing stage of an iron ore processing plant.



Fig. 1. Failed mantle liner showing macrocracks after 375 hours of service.

The designation as Grade C refers to the material specification required at procurement and should not be interpreted as confirmation of compliance with the chemical composition requirements of the standard ASTM A128/A128M [2]. Compliance was subsequently assessed based on the chemical analyses reported in Section 3.2. The processed material consisted of compact itabirite ore, characterized by high mechanical strength. The operating conditions evaluated in this study were representative of normal plant practice. Throughout the period investigated, no significant deviations in feed characteristics, crusher settings, maintenance procedures, or operating parameters were reported by the plant. The quaternary crushing feed exhibited a top size of approximately 50 mm, with 100% passing 50 mm and 97% passing 38 mm. The average feed rate was 1,256 t/h on a wet basis (1,181 t/h on a dry basis), with a solids content of 94%, corresponding to an approximate moisture content of 6%. The crusher evaluated was a Sandvik CH660 cone crusher, equipped with a B-profile mantle, MF (Medium Fine) concave, and operating at a 40 mm CSS (closed-side setting). Occasional occurrences of tramp metal were observed in the feed, which is inherent to the process; however, no crusher stalls, overload events, or associated

operational interruptions were recorded during the evaluation period. Plant operating records did not indicate abnormal feed conditions, unusual power demand, maintenance-related problems, installation deficiencies, or process disturbances that could reasonably explain the premature failures. Therefore, no evidence of significant operational deviation was identified during the investigation.

Three mantle liners suffered catastrophic fracture after 260, 375, and 560 hours of operation, respectively, and were removed from service at those times, despite the component's expected service life of approximately 800 hours under normal operating conditions. These early failures resulted in unscheduled corrective maintenance and significant operational downtime.

For material characterization and failure analysis, one sample was extracted from each liner. Each sample measured 300 × 300 mm and included, at its center, the region where macrocracks had initiated (Figure 2). All metallographic examinations, hardness measurements, tensile tests, and Charpy impact tests were performed on specimens extracted from these 300 × 300 mm sections. The crack-initiation region was intentionally positioned near the center of the extracted block to ensure that the analyzed specimens were representative of the material condition associated with the observed failure.



Fig. 2. Extracted samples (a) M1, (b) M2, (c) M3.

2.2 Methods

Chemical composition was determined by spark optical emission spectrometry (Spark-OES) using an Anacom Científica B2ADV spectrometer in accordance with ASTM E2209 [5], which is specifically applicable to the analysis of high-manganese steels. Prior to analysis, the spectrometer was calibrated using multiple high-manganese-steel reference standards with different Mn contents. This calibration procedure is performed before the chemical analysis of high-manganese steels to establish/verify the appropriate analytical response for this material class. The Mn concentrations measured in the investigated samples (10.33–11.92 wt.%) fall within the 8.0–16.2 wt.% Mn range covered by ASTM E2209 [5].

Microstructural characterization included optical microscopy after sectioning, mounting in bakelite, grinding, polishing, and etching with 2% Nital; grain size measurements were performed according to ASTM E112-13 [6] using an Olympus BX41M microscope. Fractographic and microstructural analyses were conducted with a Jeol IT-200 scanning electron microscope equipped with an Oxford EDX detector and Aztec software. Mechanical characterization comprised Charpy impact testing with a Time JB300 pendulum machine (300 J), using Type A specimens tested at 23 °C in accordance with ASTM E23-18 [7]; tensile testing was performed using an Instron 2382 universal testing machine (100 kN) under displacement control, with specimen geometry and procedures following ASTM E8/E8M-22 [8]. Hardness measurements were obtained using a Wilson 4JR Rockwell tester following ASTM E18-20 [9]. For all mechanical tests, three specimens were evaluated for each failed mantle liner, totaling nine specimens. The values reported correspond to the average results obtained from the three specimens tested for each liner. Hardness measurements were performed on sections extracted from the vicinity of the crack initiation region and correspond to bulk material rather than the worn working surface of the mantle. Tensile, impact, hardness, and microscopy specimens were extracted from the same sampled region surrounding the crack-initiation site. Because the investigation was performed on components removed from service after failure, the objective was to characterize the metallurgical condition associated with the fracture rather than to evaluate spatial property variations throughout the entire casting.

Therefore, the present analysis is representative of the metallurgical condition of the material in the vicinity of the crack-initiation region, which was intentionally selected for specimen extraction and subsequent microstructural and mechanical characterization.

3. RESULTS AND DISCUSSION

3.1 Tribosystem characterization

In cone crushers, the tribosystem governs the interaction between ore particles and liner surfaces, directly influencing crushing efficiency, wear progression, and overall equipment performance. The crushing chamber consists of two principal components: the mantle, mounted on the main shaft, and the concave, a stationary bowl liner that defines the chamber geometry. The mantle performs an eccentric gyratory motion, cyclically approaching and retreating from the concave, thereby generating continuous variations in the interfacial gap (Closed Side Setting, CSS) and subjecting incoming ore to high compressive forces [10]. This alternating movement is responsible for the primary fragmentation mechanism, in which particles are crushed predominantly by compression, complemented by bending and shearing forces within each cycle.

As the mantle moves inward, particles trapped between the opposing surfaces are fractured; when the mantle moves outward, the crushed material descends, maintaining a consistent flow of ore within the chamber. From a tribological perspective, this system operates largely under three-body abrasive wear conditions, where ore particles act as mobile abrasive bodies capable of rolling and sliding between metal surfaces rather than removing material uniformly through continuous two-body abrasion. Associated with the comminution process, compression and fragmentation of the processed material also occur simultaneously, leading to repeated indentations on the surfaces of the crusher mantle and cone. This wear mechanism aligns with established wear models for cone crushers, which indicate that particle mobility leads to episodic micro-cutting, grooving, and plastic deformation rather than constant material removal [10].

The evolution of the tribosystem has pronounced effects on operational performance. Progressive wear of the mantle and concave alters the original chamber profile, modifying ore flow patterns, increasing energy demand, and degrading product size distribution. Industrial observations show that as wear advances, geometric distortions—such as lip formation at the bottom of the mantle—can restrict the downward flow of fines, resulting in reduced throughput and unstable operating conditions. Consequently, understanding the tribosystem is essential for predicting wear progression, designing optimized chamber geometries, and implementing wear-compensation strategies to stabilize crusher performance over its service life.

Although abrasive wear is an inherent aspect of cone-crusher operation and contributed to the service degradation of the examined liners, the present investigation focuses primarily on the metallurgical and fracture-related aspects of the premature failures. Quantitative measurements of wear loss, wear volume, or wear rate were not available for the investigated components.

3.2 Chemical composition

Because the mantle liners had been procured and specified as ASTM A128/A128M [2] Grade C castings, the measured chemical compositions were compared with the compositional requirements for Grade C given in ASTM A128/A128M [2]. For Grade C, the specified composition ranges are 1.05–1.35 wt.% C, 11.5–14.0 wt.% Mn, 1.5–2.5 wt.% Cr, ≤1.00 wt.% Si, and ≤0.070 wt.% P. The comparison, presented in Table 1, shows that none of the three investigated liners fully met the Grade C chemical-composition requirements. Sample M1 contained manganese within the required range (11.92 wt.%) but exhibited a chromium content slightly below the minimum specified limit (1.41 wt.%). Samples M2 and M3 showed more pronounced deviations, with manganese contents of 10.33 wt.% and 10.85 wt.%, respectively, as well as chromium contents of 1.03 wt.% and 1.26 wt.%, both significantly below the ASTM A128/A128M requirements [2]. Therefore, all investigated liners presented compositional nonconformities that may have adversely affected their metallurgical performan

Table 1. Chemical composition (%wt) of investigated samples vs ASTM A128/A128M Grade C [2].

	%wt												
Samples	**C**	**Si**	**Mn**	**P**	**S**	**Cr**	**Ni**	**Mo**	**V**	**Ti**	**Al**	**Cu**	**Fe**
M1	1.16	0.39	11.92	0.053	ND	1.41	0.06	0.19	0.029	0.002	0.014	0.05	Bal
M2	1.12	0.66	10.33	0.052	0.003	1.03	0.05	0.16	0.025	0.004	0.031	0.04	Bal
M3	1.14	0.40	10.85	0.053	0.001	1.26	0.09	0.16	0.025	0.006	0.020	0.06	Bal
ASTM A128 Grade C [2]	**1.05-1.35**	**1.00 max**	**11.5-14.0**	**0.070 max**	**NE**	**1.5-2.5**	**NS**	**NS**	**NS**	**NS**	**NS**	**NS**	**Bal**

ND: Not Detected; NE: Not Specified; Bal: Balance

Although the deviation observed for sample M1 was relatively small and restricted to chromium content, the deficiencies identified in samples M2 and M3 were substantial enough to alter the expected behavior of Hadfield steel under severe impact-abrasion conditions. Since the three liners were installed under similar operating conditions and all failed prematurely, the compositional deviations provide important evidence that metallurgical factors contributed to the reduced service life. In particular, the insufficient manganese levels observed in M2 and M3 may have reduced austenite stability and potentially affected the material's capacity to develop work hardening during service.

Sub-standard Mn and Cr contents directly compromise properties related to abrasive wear and impact resistance. Manganese is essential for stabilizing the austenitic microstructure responsible for the toughness, ductility, and work-hardening behavior characteristic of Hadfield steels. Metallurgical studies show that maintaining Mn above 10% is crucial for impact resistance, microstructural stability, and sustained work-hardening capacity during service. Optimal mechanical performance is typically observed around 12% Mn, and steels modified to contain higher Mn (≈18%) and Cr (≈2%) exhibit significant improvements in wear life under demanding crusher operating conditions [11].

When Mn falls near the lower threshold, the material shows reduced tensile strength, lower ductility, diminished crack-resistance, and accelerated mechanical degradation during crushing. When the Mn content approaches the lower threshold, the austenitic phase becomes metastable, reducing the stacking fault energy and destabilizing the deformation mechanisms responsible for work hardening. Under the severe impact and compressive loading conditions typical of crushing operations, this metastability promotes deformation-induced martensitic transformation instead of mechanical twinning. The formation of hard and brittle martensite islands within the austenitic matrix leads to reduced ductility, lower crack-propagation resistance, and accelerated mechanical degradation, ultimately favoring premature fracture of the crusher liners [12,13]. Similarly, chromium contents below approximately 2% reduce the stability of carbides and the steel's resistance to abrasive mechanisms such as gouging, micro-cutting, and surface fatigue. Engineering analyses confirm that steels containing around 2% Cr provide superior wear resistance and longer operational life when used in cone-crusher liners [11].

Therefore, deviations from the ASTM A128/A128M Grade C specification [2], particularly in Mn and Cr, may reduce austenitic stability and may adversely affect the material's ability to develop work hardening during service. Although surface work hardening was not directly evaluated in the present investigation, such compositional deviations are reported in the literature to increase susceptibility to crack formation and wear, potentially contributing to reduced service life.

3.3 Microstructure (optical microscopy)

Optical microscopy of the three samples (M1, M2, M3) revealed the presence of numerous micro-shrinkage defects (red arrows) and carbide particles within the material, particularly in the central regions, as highlighted in Figures 3, 4 and 5. These carbides were observed both as isolated precipitates and as elongated or irregular clusters distributed within the grains and along grain boundaries. The numerous carbide particles observed within the cores of all samples suggest incomplete carbide dissolution during heat treatment, consistent with the known behavior of Hadfield steels, which may retain carbide precipitates when solution treatment is insufficient to achieve complete dissolution [14].

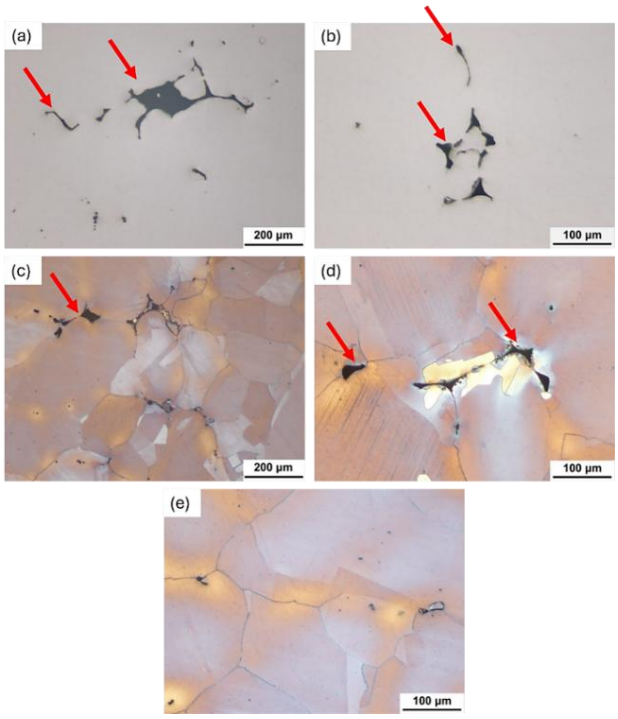


Fig. 3. Optical micrographs of M1: (a) and (b) unetched condition (red arrows highlighted defects); (c) and (d) etched condition (red arrows highlighted defects); and (e) core region.

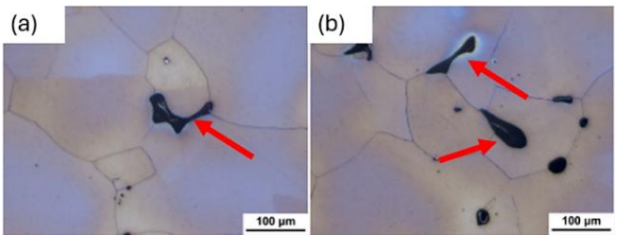


Fig. 4. Optical micrographs of M2: (a) etched (red arrows highlighted defects) and (b) core region (red arrows highlighted defects).

Defects along grain boundaries—such as micro shrinkage (red arrow), carbide networks, and microcracks—were also frequently detected. These discontinuities create preferential paths for crack propagation, consistent with observations in heavily loaded manganese steel components where crack networks originate at grain-boundary defects and propagate due to repeated strain localization [15]. In Hadfield steel castings, micro-shrinkage defects may form during the final stages of solidification due to inadequate feeding of interdendritic liquid metal. The combination of high alloy content, a relatively broad freezing range, and volumetric contraction during solidification increases the tendency for local shrinkage formation. When present near grain boundaries, these defects reduce local mechanical integrity and create stress-concentration sites that facilitate crack initiation and propagation. Under the severe impact and compressive loading conditions experienced by crusher mantle liners, micro-shrinkage defects can therefore contribute significantly to premature failure.

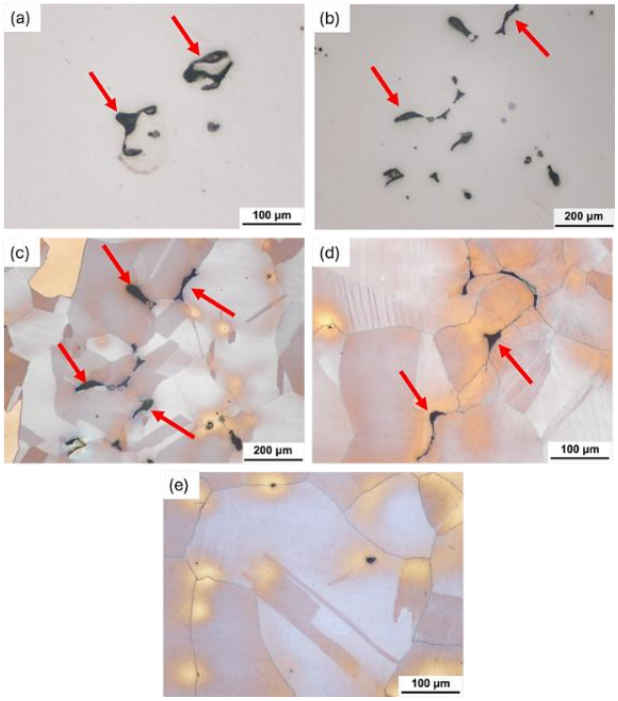


Fig. 5. Optical micrographs of M3: (a) and (b) unetched condition (red arrows highlighted defects); (c) and (d) etched condition (red arrows highlighted defects); and (e) core region.

Average grain-size measurements performed according to ASTM E112 revealed ASTM grain-size numbers G = 1 for all samples, M1, M2, and M3. No substantial differences in grain size were observed among the analyzed samples, suggesting that the principal microstructural differences were associated with carbide precipitation and grain-boundary defects rather than grain coarsening.

Lage et al. [1] studied a pair of CH660 crusher liners used in quaternary crushing, which were removed after 800 hours of service. The authors observed carbide films at 2000x magnification (Figure 6)—features that were not detectable at 100x. Although this defect is not of major significance when detected at 2000x magnification, it is an issue that warrants attention and could be improved in the casting process.

The identified carbides may act as local stress concentrators and thereby facilitate crack initiation under cyclic loading. This mechanism aligns with fatigue studies showing that local

carbon segregation and carbide formation significantly influence crack initiation behavior in austenitic manganese steels. In addition to intragranular carbides, grain-boundary carbides were observed in all samples, forming continuous or semi-continuous films. Such microstructural features are well-known to reduce grain-boundary cohesion and promote intergranular embrittlement, especially when carbide coverage becomes significant. Literature demonstrates that grain-boundary carbides in Hadfield steels severely degrade impact toughness and drastically increase susceptibility to intergranular cracking [15-16].

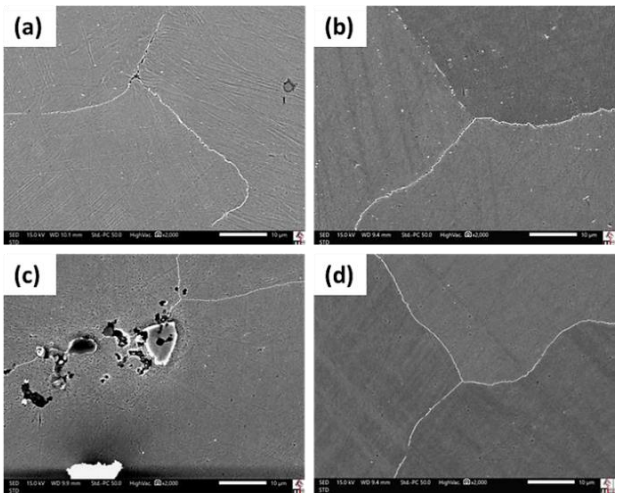


Fig. 6. Microstructure of samples observed via SEM at 2000x magnification: (a) Upper mantle; (b) Lower mantle; (c) Upper concave section; (d) Lower concave section. Adapted from Lage et al [1].

This microstructural condition is commonly associated with slow cooling during sand casting or unintentional reheating in the range of 400–800 °C, which promotes carbide precipitation along grain boundaries and reduces toughness. Similar findings have been reported in engineering components subject to heavy cyclic loading, where manufacturing-induced microstructural defects significantly shorten service life by accelerating fatigue crack formation [15].

Overall, the optical microscopy results indicate that all samples exhibit microstructural features detrimental to mechanical integrity—particularly extensive carbide precipitation and grain-boundary defects—conditions known to reduce ductility, toughness, and wear resistance, and therefore accelerate failure under impact and abrasive service.

The present investigation focused primarily on identifying microstructural features associated with premature failure. Although micro shrinkage and carbide precipitation was clearly observed, quantitative measurements of carbide area fraction, grain-boundary coverage, and particle-size distribution were not performed. Therefore, the discussion is based on qualitative microstructural observations combined with the mechanical and fractographic evidence obtained from the failed liners.

3.4 Scanning electron microscopy - Service fracture analysis

The SEM investigation provided high-resolution insights into the fracture surfaces of samples M1, M2, and M3, enabling a detailed examination of the crack-nucleation regions and the dominant fracture mechanisms. Figures 7, 8 and 9, highlight distinct microstructural features associated with each sample.

In samples M1 and M3, the fracture surfaces exhibited a thick oxide layer, characterized by extensive surface roughness, fragmentation, and an absence of metallic features typically associated with fatigue crack propagation. The pronounced oxidation obscures potential striation patterns, making it impossible to determine whether fatigue mechanisms contributed to the early stages of crack growth. This observation is supported by the compositional analysis shown in the EDS spectrum, which revealed a high oxygen content (~35%) alongside iron as the major constituent, consistent with the formation of complex iron oxides. Although substantial oxide formation was detected on the fracture surfaces, the present results do not allow oxidation to be identified as the primary crack-initiation mechanism. The observed oxidation may have developed during crack propagation in service or after the fracture surfaces became exposed. Therefore, oxidation should be interpreted as an important fractographic observation rather than direct evidence of the origin of failure. The presence of extensive oxidation indicates that the fracture surfaces were exposed to an oxidizing environment for a sufficient period of time. However, the available evidence does not allow determination of whether oxidation occurred prior to crack propagation, during crack growth, or after fracture-surface exposure.

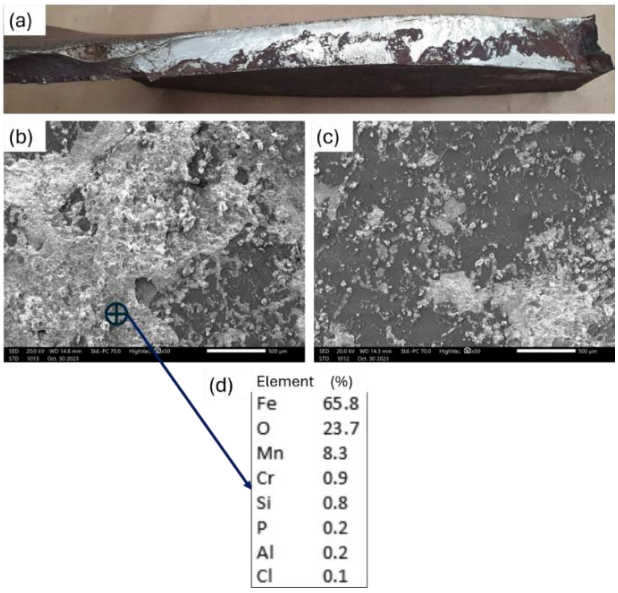


Fig. 7. SEM analysis showing crushing and a large amount of oxides in the nucleation region of the crack in sample M1: (a) fractured region; (b) and (c) surface fracture and (d) EDS results.

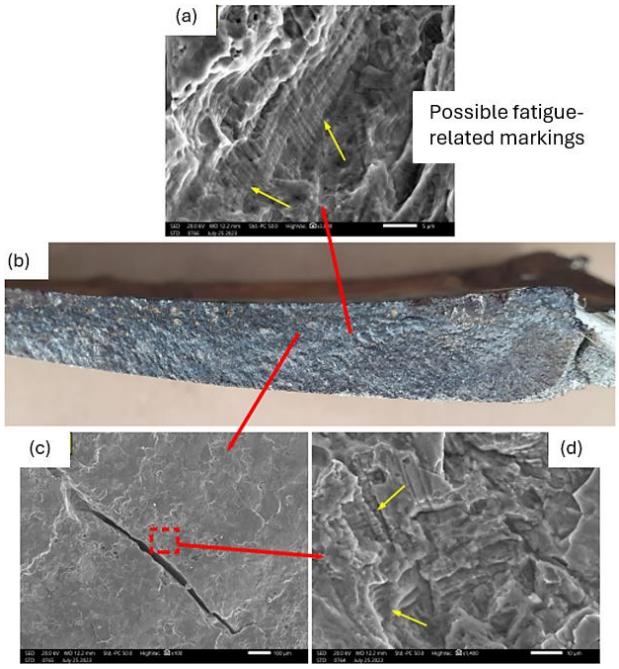


Fig. 8. SEM fractography of sample M2 showing parallel surface markings suggestive of possible fatigue-assisted crack propagation: (a) possible fatigue-related markings (yellow arrows); (b) fractured region; (c) and (d) fracture surface details.

In contrast, sample M2 exhibited localized parallel surface markings that may be associated with fatigue-assisted crack propagation and displayed features suggestive of fatigue striations as shown in Figure 8. Although these features suggest progressive crack growth under cyclic loading, their morphology indicates sustained localized plastic deformation during propagation, behavior expected in materials that retain some degree of ductility. The observed surface markings are consistent with progressive crack advancement under cyclic loading and therefore suggest that fatigue may have contributed to the crack-propagation process prior to final fracture. This finding aligns with classical descriptions of fatigue striation formation, which attribute these features to the plastic blunting and re-sharpening of the crack tip during successive loading cycles. The observed fracture-surface markings are consistent with possible fatigue-assisted crack propagation in M2. However, because definitive fatigue features such as well-defined striations could not be conclusively identified, these observations should be interpreted as suggestive rather than conclusive evidence of fatigue. This distinguishes M2 from the oxidation-dominated fracture surfaces observed in M1 and M3.

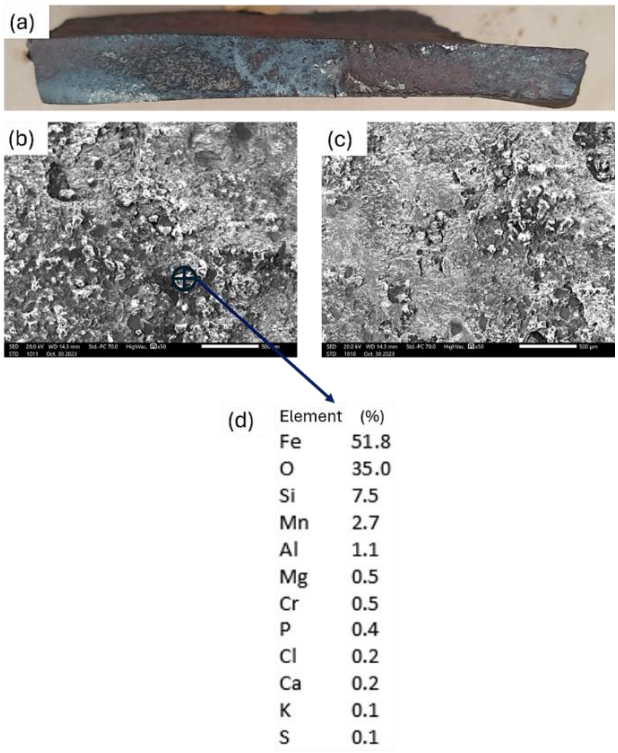


Fig. 9. SEM analysis showing crushing and a large amount of oxides in the nucleation region of the crack in sample M3: (a) fractured region; (b) and (c) SEM surface fracture and (d) EDS results.

The observations described above correspond exclusively to fracture surfaces generated during service in the crusher environment. Consequently, the identified oxidation features, fatigue markings, and crack-propagation characteristics are directly associated with the field failure of the mantle liners.

The different crack propagation mechanisms observed among the liners may be associated with local microstructural heterogeneities arising from casting and heat-treatment variations. M1 and M3 show fracture surfaces containing extensive oxidation and brittle intergranular features. However, the temporal relationship between oxidation and crack propagation could not be established from the available evidence, whereas M2 exhibited localized markings consistent with possible fatigue-assisted crack propagation. These observations suggest that relatively small metallurgical variations can significantly influence crack development in service.

Although a direct reference specimen was not available, a useful benchmark is provided by the study of Lage et al. [1], which evaluated Hadfield-steel liners operating in the same CH660 crusher model under comparable quaternary crushing conditions and reported service lives close to the expected 800 h. This comparison provides additional context for interpreting the premature failures investigated in the present work.

3.5 Fractography of mechanical-test specimens

Additional SEM examinations were performed on fracture surfaces generated during tensile and Charpy impact testing (Figures 10–12). Unlike the service fractures discussed previously, these surfaces were produced under controlled laboratory conditions and therefore should be interpreted independently. The objective of these analyses was not to reproduce the service failure mechanism, but rather to evaluate the intrinsic fracture behavior of the material and the effect of the observed microstructural degradation on mechanical performance. Faceted surfaces and crack propagation along grain boundaries were consistently observed, indicating a loss of cohesion at these interfaces. Such fracture morphology is consistent with conditions where grain boundaries become mechanically weaker than the grain interiors, causing cracks to follow the energetically favorable intergranular path. This mechanism supports prior microstructural findings of carbide networks and grain-boundary heterogeneities, like micro shrinkage, which can significantly reduce toughness and promote intergranular embrittlement.

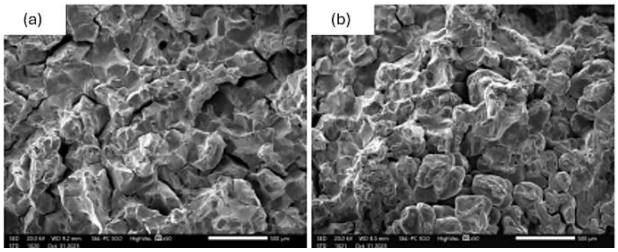


Fig. 10. SEM analysis of tensile and impact test specimens from sample M1: (a) impact test and (b) tensile stress test.

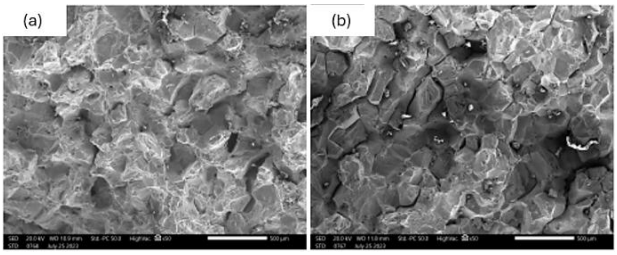


Fig. 11. SEM analysis of tensile and impact test specimens from sample M2: (a) impact test and (b) tensile stress test.

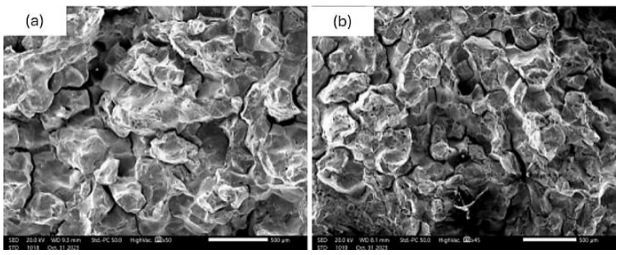


Fig. 12. SEM analysis of tensile and impact test specimens from sample M3: (a) impact test and (b) tensile stress test.

Although tensile and impact tests impose loading conditions that differ substantially from those experienced in service, the predominance of intergranular fracture observed in these specimens provides additional evidence of weakened grain-boundary cohesion. However, these laboratory observations are not interpreted as direct representations of the crack-growth mechanisms operating in the crusher liners during service.

Overall, SEM examination revealed distinct fracture-surface characteristics among the investigated liners. Extensive oxidation was observed in M1 and M3, although its temporal relationship with crack propagation could not be established. In M2, localized markings were consistent with possible fatigue-assisted crack propagation. Separately, the fractography of tensile and impact specimens revealed a strong

tendency toward intergranular fracture, providing independent evidence of reduced grain-boundary cohesion. Together, these observations support the conclusion that metallurgical degradation contributed significantly to the premature failures, while acknowledging that service-related and laboratory-generated fracture surfaces represent distinct loading histories and fracture processes.

3.6 Charpy impact tests and hardness measurements

The Charpy impact energy values obtained for samples M1, M2, and M3 were 56.7 J, 82.0 J, and 48.0 J, respectively, as shown in Table 2. These results indicate relatively low impact toughness when compared with values commonly reported for properly solution-treated Hadfield steels (110-180 J) [1,3,4,14]. However, impact-energy values reported in the literature are strongly influenced by testing conditions, including specimen geometry, notch configuration, testing temperature, casting condition, section thickness, and alloy composition. Therefore, literature values should be interpreted as a general reference rather than as strict performance limits. Nevertheless, considering that the present specimens were tested at room temperature using standard ASTM E23 Charpy V-notch specimens, the measured energies remain indicative of reduced toughness when compared with values typically reported for solution-treated austenitic manganese steels.

Furthermore, the mechanical behavior of Hadfield steel is highly dependent on the effectiveness of solution treatment, the resulting carbide distribution, and the overall casting quality. Materials containing grain-boundary carbide precipitates, micro-shrinkage defects, solidification-related segregation, or compositional deviations from ASTM A128/A128M requirements [2] often exhibit significantly lower impact toughness than fully solution-treated alloys. In particular, micro-shrinkage defects formed during the final stages of solidification act as stress concentrators, whereas grain-boundary carbides reduce local cohesion and promote intergranular cracking. Therefore, the reduced impact energies observed in this study should be interpreted together with the microstructural evidence presented in Sections 3.2 and 3.3.

This decrease in impact energy is consistent with the microstructural findings presented in Section 3.3, where all samples exhibited considerable amounts of micro-shrinkage and carbides along grain boundaries. The presence of micro-shrinkage and grain-boundary carbides reduces local cohesion between adjacent grains, creating preferential sites for crack nucleation. As a result, even relatively low impact energies may trigger the initiation and rapid propagation of microcracks along weakened interfaces, ultimately lowering the overall fracture resistance of the material.

Among the investigated samples, M2 exhibited the highest Charpy impact energy (82.0 ± 4.0 J), compared with 56.7 ± 8.1 J for M1 and 48.0 ± 7.2 J for M3. This result indicates that M2 had greater impact-energy absorption capacity under the test conditions used in this study. Nevertheless, the microstructural examination of M2 still revealed grain-boundary carbides and micro-shrinkage defects. Therefore, the Charpy result should be interpreted together with the microstructural and fractographic evidence rather than used independently to classify the material condition.

Overall, the Charpy results, considered together with the microstructural and fractographic observations, are consistent with reduced grain-boundary cohesion associated with carbide precipitation and micro-shrinkage defects. These features may have contributed to the reduced impact-energy absorption observed particularly in M1 and M3.

The hardness results obtained for samples M1, M2, and M3 are presented in Table 2. The average hardness values were 93.4 HRB for M1, 91.0 HRB for M2, and 92.2 HRB for M3, falling within the range commonly reported for Hadfield steel. Because the measurements were performed on specimens extracted from regions near the crack-initiation sites rather than directly from the worn service surfaces, the results should be interpreted as representative of the bulk material condition. Although the measured hardness levels are consistent with those often associated with non-work-hardened Hadfield steel, the present data do not allow a definitive assessment of the presence or extent of surface work hardening developed during service. Such an evaluation would require direct surface-hardness measurements, hardness-depth profiles, or microhardness mapping from the surface toward the core, which were beyond the scope of the present investigation.

Table 2. Rockwell hardness (HRB) and Charpy V-notch impact energy results reported as mean ± standard deviation (n = 3).

Sample	Hardness (HRB)	Impact energy (J)
M1	93.4 ± 0.5	56.7 ± 8.1
M2	91.0 ± 0.7	82.0 ± 4.0
M3	92.2 ± 0.8	48.0 ± 7.2

3.7 Tensile tests

The tensile-test results for samples M1, M2, and M3 are presented in Table 3. The reported values correspond to the average results obtained from three specimens tested for each liner. All three samples exhibited relatively low ultimate tensile strength (UTS) in combination with moderate to high ductility, as reflected by the elongation and reduction of area.

All three samples exhibited relatively low ultimate tensile strength (UTS) in combination with measurable ductility, as indicated by the elongation and reduction of area. The measured yield strengths ranged from 398.1 to 440.4 MPa. Published mechanical-property values for Hadfield steels vary considerably depending on chemical composition, casting condition, heat-treatment practice, section thickness, and testing methodology. Therefore, literature values are used only as a general reference, and the tensile behavior observed here is interpreted primarily in conjunction with the measured chemical compositions and microstructural characteristics. The tensile properties obtained in the present investigation were therefore interpreted primarily in relation to the measured chemical composition and observed microstructure rather than through direct comparison with a single literature range. The presence of grain-boundary carbides, micro-shrinkage defects, and compositional deviations from ASTM A128/A128M Grade C [2] are likely to have influenced the tensile response and contributed to the observed mechanical performance. The yield-strength values obtained for the investigated samples were higher than those commonly reported for solution-treated Hadfield steels. However, yield strength is influenced by several factors, including chemical composition, microstructural condition, carbide precipitation, and casting characteristics. Therefore, these values should be interpreted together with the microstructural observations rather than as evidence of a specific fracture-mode transition. The relatively elevated yield strength values may be associated with microstructural heterogeneities caused by carbide precipitation and local compositional variations. Although surface work hardening could not be assessed from the present bulk-hardness measurements, these metallurgical features can increase resistance to initial plastic deformation while simultaneously reducing toughness.

Table 3. Tensile test results reported as mean ± standard deviation (n = 3).

Sample	Elongation (%)	Reduction of Area (%)	Yield strength (Mpa)	UTS (Mpa)
M1	13.6 ± 1.1	15.3 ± 2.1	426.2 ± 4.4	570.9 ± 5.5
M2	12.8 ± 2.5	17.4 ± 0.7	398.1 ± 6.3	571.5 ± 8.8
M3	25.5 ± 0.9	25.6 ± 1.3	440.4 ± 5.1	691.6 ± 6.7

Se = 0.2% offset yield strength, Sr = ultimate tensile strength, A = elongation, RA = reduction of area.

In all cases, the relatively low UTS values suggest a loss of mechanical performance, consistent with the microstructural degradation observed in earlier analyses. As highlighted previously, the presence of grain-boundary carbides, microstructural heterogeneities, and signs of embrittlement—especially in samples M1 and M3—can contribute to reduced tensile capacity by undermining the cohesive strength of the grain boundaries and facilitating premature crack initiation under monotonic loading.

Sample M3 exhibited the highest elongation (25.5%) and reduction of area (25.6%), indicating a more substantial capacity for uniform plastic deformation. However, even in this case, the ultimate tensile strength remained below what would be expected for a fully solution-treated and structurally stable Hadfield steel. This behavior reinforces the conclusion that all samples experienced some degree of microstructural destabilization, consistent with the prior findings from optical and electron microscopy.

Overall, the tensile-test results indicate that the materials were mechanically affected by metallurgical degradation. Although measurable plastic deformation occurred during tensile loading, as indicated by the elongation and reduction-of-area values, the fractographic analyses revealed that final fracture was strongly influenced by intergranular crack propagation. Consequently, the tensile results should be interpreted as evidence that global plastic deformation coexisted with local fracture mechanisms associated with grain-boundary weakening.

The combination of moderate tensile ductility and intergranular fracture is not necessarily contradictory. Tensile elongation reflects the global deformation accumulated throughout the specimen gauge length prior to failure, whereas SEM observations describe the local fracture mechanism operating immediately before final rupture. Consequently, a material may exhibit appreciable macroscopic plastic deformation during tensile loading while still failing through intergranular crack propagation if grain-boundary cohesion is locally reduced by carbide precipitation, micro-shrinkage defects, or compositional heterogeneities.

A useful benchmark can be established by comparing the present results with the crusher liners investigated by Lage et al. [1], which operated under similar quaternary crushing conditions and achieved the expected service life of approximately 800 h. In contrast, the liners analyzed in the present study failed after only 260, 375 and 560 h of operation. Although both studies reported the presence of carbide films, the liners evaluated by Lage et al. [1] did not exhibit the extensive grain-boundary carbide precipitation, compositional deviations, reduced impact toughness and intergranular fracture features observed in the present investigation. The substantially shorter service life observed here therefore suggests that the combined effect of chemical nonconformities and microstructural defects significantly accelerated damage accumulation and crack propagation.

Although the metallurgical evidence consistently indicates degraded material condition in all analyzed liners, the present investigation was focused on component characterization after failure. Although no evidence of abnormal operating conditions was identified during the evaluation period, the possible influence of local operational, geometric, or residual-stress-related factors cannot be completely excluded.

Table 4 shows that all investigated mantle liners exhibited compositional deviations from ASTM A128/A128M Grade C [2] requirements, grain-boundary carbide precipitation, and evidence of microstructural degradation. However, a straightforward correlation between a single metallurgical parameter and service life was not observed. Sample M1, which exhibited the shortest service life (260 h), showed grain-boundary carbides, micro-shrinkage defects, and extensive oxidation. Sample M2 achieved an intermediate life (375 h) and exhibited the highest impact toughness among the investigated liners, together with fracture features compatible with fatigue-assisted crack propagation. Sample M3 exhibited the longest service life (560 h), despite presenting metallurgical deficiencies similar to those observed in the other samples. These results suggest that premature failure was influenced by the combined effect of multiple metallurgical factors rather than by a single isolated defect.

Table 4. Summary of service life, mechanical properties and principal metallurgical observations.

Sample	Service life (h)	Mn (%)	Cr (%)	Hardness (HRB)	Impact Energy (J)	Yield Strength (MPa)	UTS (MPa)	Main observations
M1	260	11.92	1.41	93.4	56.7	426.2	570.9	Grain-boundary carbides, micro-shrinkage, extensive fracture-surface oxidation
M2	375	10.33	1.03	91.0	82.0	398.1	571.5	Grain-boundary carbides, micro-shrinkage, markings consistent with possible fatigue-assisted crack propagation
M3	560	10.85	1.26	92.2	48.0	440.4	691.6	Grain-boundary carbides, micro-shrinkage, extensive fracture-surface oxidation

4. CONCLUSION

Based on the chemical, microstructural, mechanical, and fractographic characterization of samples M1, M2, and M3, several conclusions can be drawn regarding the metallurgical conditions associated with the premature failures of the investigated mantle liners. Because no reference liner in satisfactory service condition was available for direct comparison, the conclusions are based on the combined interpretation of the experimental results, applicable material specifications, published literature, and previously reported field performance of similar crusher liners.

Although the investigated mantle liners were procured and specified as ASTM A128/A128M Grade C [2] castings, chemical analysis revealed that none fully met the compositional requirements of this grade. Sample M1 exhibited a manganese content within the specified range but a chromium content slightly below the minimum requirement, whereas M2 and M3 exhibited both manganese and chromium contents below the specified ranges. These compositional deviations indicate that the supplied materials did not fully satisfy the intended Grade C chemical specification.

Optical microscopy revealed grain-boundary carbide precipitation and micro-shrinkage defects in all investigated samples. These microstructural features are potentially detrimental to grain-boundary cohesion and may provide preferential sites for crack initiation and propagation. However, carbide area fraction, grain-boundary coverage, and particle-size distribution were not quantitatively determined. Therefore, although carbide precipitation is considered an important metallurgical factor associated with the observed degradation, its individual contribution to the premature failures cannot be quantified from the present results.

SEM examination of the service-fracture surfaces revealed different features among the investigated liners. Samples M1 and M3 exhibited extensive surface oxidation, which obscured the underlying fracture morphology and limited detailed fractographic interpretation. Importantly, the temporal relationship between oxidation and crack propagation could not be established. Therefore, the observed oxidation cannot be conclusively identified as a cause of crack initiation or propagation and may have developed before, during, or after fracture-surface exposure. In contrast, sample M2 exhibited markings suggestive of possible fatigue-assisted crack propagation. These features suggest that cyclic loading may have contributed to crack propagation in M2; however, they are not considered definitive evidence of fatigue.

Mechanical testing provided additional evidence of differences in material condition among the investigated liners. M1 and M3 exhibited lower Charpy impact-energy absorption than M2, while fractographic examination of the laboratory-generated tensile and impact fracture surfaces revealed a pronounced tendency toward intergranular crack propagation. These observations, considered together with the grain-boundary carbide precipitation and micro-shrinkage defects, indicate locally weakened grain-boundary cohesion.

The bulk hardness measurements obtained near the crack-initiation regions were consistent with hardness levels generally associated with non-work-hardened Hadfield steel. However, because the measurements were not performed directly on the worn service surfaces and no hardness-depth profiles or microhardness mapping were obtained, the presence and extent of surface work hardening developed during service could not be established. Consequently, the present hardness results should not be interpreted as evidence that surface work hardening did not occur during operation.

Overall, the combined evidence indicates that deviations from the intended chemical composition, grain-boundary carbide precipitation, micro-shrinkage defects, and associated degradation of mechanical performance were important metallurgical factors associated with the premature failure of the investigated mantle liners. Nevertheless, because carbide precipitation and surface work hardening were not quantitatively characterized, and because the temporal role of oxidation could not be established, the individual contribution of these factors to the failure process cannot be quantified conclusively. Similarly, the fracture markings observed in M2 indicate possible fatigue-assisted crack growth but do not constitute definitive proof of fatigue.

These findings suggest the importance of improved manufacturing and quality-control practices for Hadfield-steel crusher liners. Recommended measures include verification of chemical composition against the specified ASTM A128/A128M [2] grade prior to acceptance, appropriate control of solution heat treatment and quenching conditions, optimization of casting and feeding practices to minimize shrinkage defects, and metallographic inspection for detrimental grain-boundary carbide precipitation. Such measures may reduce the occurrence of metallurgical defects associated with premature fracture and improve the reliability of mantle liners in service.

Acknowledgement

The authors acknowledge Vale and the Vale Institute of Technology for their support and encouragement, as well as the Materials Institute of Brazil (MIB) for the characterization analyses performed.

REFERENCES

[1] W. C. Lage, J. Penagos, and G. Tressia, "Tribological study of fourth-stage crusher coatings applied in an iron ore processing plant", *Tribology International*, vol. 190, 109021, Dec. 2023, doi: 10.1016/j.triboint.2023.109021.

[2] *Standard Specification for Steel Castings, Austenitic Manganese*, ASTM A128/A128M-19, ASTM International, West Conshohocken, PA, USA, 2019, doi: 10.1520/A0128_A0128M-19.

[3] N. L. Santos, D. Todorov, A. H. Cavalcanti, and R. Fuoco, "Effect of carbide reprecipitation on the toughness of Hadfield austenitic manganese steel". *Transactions of the American Foundry Society*, vol. 118, pp. 397-412, Oct. 2010.

[4] O. A. Zambrano, G. Tressia, and R. M. Souza, "Failure analysis of a crossing rail made of Hadfield steel after severe plastic deformation induced by wheel-rail interaction", *Engineering Failure Analysis*, vol. 115, Art. No. 104621, Sep. 2020, doi: 10.1016/j.engfailanal.2020.104621.

[5] *Standard Test Method for Analysis of High Manganese Steel by Spark Atomic Emission Spectrometry*, ASTM E2209-22, ASTM International, West Conshohocken, PA, USA, 2022, doi: 10.1520/E2209-22.

[6] *Standard Test Methods for Determining Average Grain Size*, ASTM E112-13, ASTM International, West Conshohocken, PA, USA, 2013, doi: 10.1520/E0112-13.

[7] *Standard Test Methods for Notched Bar Impact Testing of Metallic Materials*, ASTM E23-18, ASTM International, West Conshohocken, PA, USA, 2018, doi: 10.1520/E0023-18.

[8] *Standard Test Methods for Tension Testing of Metallic Materials*, ASTM E8/E8M-22, ASTM International, West Conshohocken, PA, USA, 2022, doi: 10.1520/E0008_E0008M-22.

[9] *Standard Test Methods for Rockwell Hardness of Metallic Materials*, ASTM E18-20, ASTM International, West Conshohocken, PA, USA, 2020, doi: 10.1520/E0018-20.

[10] Z. Zhang, T. Ren, and J. Cheng, "Constant wear criterion for optimization of the crushing chamber of cone crushers", *Minerals*, vol. 12, no. 7, Art. No. 807, Jun. 2022, doi: 10.3390/min12070807.

[11] M. Lindroos, M. Apostol, V. Heino, K. Valtonen, A. Laukkanen, K. Holmberg, and V. T. Kuokkala, "The deformation, strain hardening, and wear behavior of chromium-alloyed Hadfield steel in abrasive and impact conditions", *Tribology Letters*, vol. 57, no. 3, 24, Jan. 2015, doi: 10.1007/s11249-015-0477-6.

[12] Y. N. Petrov, V. G. Gavriljuk, H. Berns, and F. Schmalt, "Surface structure of stainless and Hadfield steel after impact wear", *Wear*, vol. 260, no. 6, pp. 687-691, Mar. 2006, doi: 10.1016/j.wear.2005.04.009.

[13] J. Tianfu, and Z. Fucheng, "The work-hardening behavior of medium manganese steel under impact abrasive wear condition", *Materials Letters*, vol. 31, no. 3–6, pp. 275-279, Jun. 1997, doi: 10.1016/S0167-577X(96)00293-5.

[14] R. Zavadil, and S. Kuyucak, "Microstructure versus impact toughness relationship in Hadfield's austenitic manganese steel", *Microscopy and Microanalysis*, vol. 8, pp. 1142–1143, Aug. 2002, doi: 10.1017/S1431927602104880.

[15] G. Tressia, T. Tepedino, M. Masoumi, and J. I. Pereira, "Microstructural evolution and strain-hardening behavior in Hadfield steel railway crossings", *Tribology in Industry*, vol. 46, no. 4, pp. 639–650, Dec. 2024, doi: 10.24874/ti.1744.08.24.10.

[16] S. Dhar, H.K. Danielsen, S. Fæster, C. Rasmussen, Y. Zhang, and D. J. Jensen, "Crack formation within a Hadfield manganese steel crossing nose", *Wear*, vols. 438–439, 203049, Nov. 2019, doi: 10.1016/j.wear.2019.203049.